Future decline of Antarctic Circumpolar Current due to polar ocean freshening

Taimoor Sohail,[1,2*] Bishakhdatta Gayen,[3,4,5*] and Andreas Klocker[6]

[1]School of Mathematics and Statistics, University of New South Wales, Sydney, Australia
[2]Australian Center for Excellence in Antarctic Science, University of New South Wales, Sydney, Australia
[3]Department of Mechanical Engineering, University of Melbourne, Melbourne, Australia
[4]Centre for Atmospheric and Oceanic Sciences, Indian Institute of Science, Bengaluru, India
[5]Australian Center for Excellence in Antarctic Science, University of Melbourne, Melbourne, Australia
[6]NORCE Norwegian Research Centre, Bjerknes Centre for Climate Research, Bergen, Norway

*To whom correspondence should be addressed;
E-mail: t.sohail@unsw.edu.au and bishakhdatta.gayen@unimelb.edu.au.

The Antarctic Circumpolar Current is the world's strongest ocean current. This vast current system is linked to ocean overturning and is pivotal to the uptake of ocean heat and CO_2. The strength of the Antarctic Circumpolar Current has varied across Earth's past climates, but the exact drivers of this change remain elusive. Ocean models have not been able to adequately resolve eddies and dense shelf water formation processes that control current strength. Here, we assess a global ocean model which resolves such processes to diagnose

the impact of future thermohaline and wind conditions on the Antarctic Circumpolar Current. This model suggests the strength of the Antarctic Circumpolar Current will decline by up to $\sim 20\%$ by 2050. This decline is supported by simple scaling theory, and is driven by ice shelf melting, which weakens the density gradient historically supported by surface temperature. Such a decline in transport would have critical implications for the global ocean circulation, and hence, Earth's climate system.

Introduction

The Southern Ocean is in a state of rapid change. Satellite observations reveal that the Antarctic ice sheet is losing mass at an accelerating pace, releasing large amounts of freshwater into the ocean along the Antarctic coast (*1–3*). Sea ice extent, which was slightly increasing until 2016, has since rapidly declined (*4*). In 2023, sea ice extent dropped to its lowest value since the advent of satellite observations (*5*). Changes in sea ice formation and melting are linked to the formation of Antarctic Bottom Water (AABW (*6–8*)), which supports the absorption of heat and carbon from the atmosphere into the deep ocean, and occupies 30-40% of volume of the global ocean (*9*). Past research has found that the formation of AABW in the Weddell Sea has reduced by 30% since 1992 as a result of changes in winds and ice melt (*7*). One of the pressing questions arising from these observed changes to the Southern Ocean is how the Antarctic Circumpolar Current (ACC) will respond.

The ACC has an observed transport of about 173 Sverdrups (1 Sverdrups = 10^6 m^3/s) (*10*), making it the world's strongest ocean current. The ACC is the only current which encircles the planet without encountering continental boundaries, and also supports the global-scale overturning circulation among the three major ocean basins (*11*). ACC transport is constrained by geostrophic balance due to the thermal wind relationship, which is a function of the meridional

and vertical density distribution throughout the Southern Ocean (*12, 13*). The configuration of these density layers is subject to alterations by surface winds as well as by salinity and temperature exchanges at the surface (*14, 15*), all of which are subject to rapid changes due to ongoing climate change (*16–20*).

Dominant westerly winds, a characteristic feature of the Southern Ocean, induce a northward Ekman transport that tends to intensify the inclination of density layers, steepening the depth-variable meridional density gradient. However, this process is counteracted by enhanced baroclinic eddies and convective mixing, together moderating the meridional density gradient and compensating transport (*14, 21–23*). On the other hand, the response of the ACC to variations in the surface buoyancy distribution (i.e., heat or freshwater fluxes) is also critical and has been influenced by past climatic changes (*24, 25*).

The ACC is also intimately linked to Antarctic Bottom Water formation along the Antarctic margins. Turbulence-resolving direct numerical simulations (*13, 26, 27*) and idealised simulations with an eddying primitive equation model (*28*) have shown that convection around the Antarctic continent, which feeds the AABW without the requirement of wind forcing, could lead to a circumpolar current similar to the ACC. This is consistent with idealised case study from a reduced gravity model where the initiation of AABW formation leads to a large increase in zonal transport (*29*). These results suggest that a change in convection around the Antarctic, which is closely tied to meltwater and sea-ice production around the Antarctic continent (*30*), could directly change the ACC. In recent decades, AABW formation has been observed to decline significantly (*31*), and freshening by glacial meltwater has played a crucial role in reducing the convection that feeds AABW formation (*30*). Recent high-resolution modelling by (*32*), found that the AABW may decline by 42% by 2050 in response to a constant meltwater perturbation from the Shared Socioeconomic Pathway 5-8.5 future projection in CMIP6. If the link between AABW formation and thermal wind transport is apparent in the real ocean, this would

suggest that the ACC is set for a long-term decline in strength.

A comprehensive assessment of historical observations and climate models by (*33*) recently found that zonal transport in the Southern Ocean has *accelerated* in past decades. This acceleration has so far been attributed to enhanced meridional temperature gradients in the region, and is isolated to a relatively narrow band centered at 52°S. ACC transport through the Drake Passage, on the other hand, has remained unchanged between 2005 and 2019, suggesting that the zonal transport acceleration seen by (*33*) has not influenced the ACC in the Drake Passage (*34*). It is still unknown how enhanced ice shelf melting, which will flux enormous volumes of freshwater into the Southern Ocean, will disrupt the recent acceleration of zonal transport or the relatively stable ACC in the future. In order to explore this question, we use an eddy-resolving global ice-ocean model to explore the impact of projected surface freshwater and temperature fluxes on the zonal transport in the Southern Ocean, sourced from (*32*) and (*35*). Our results show that the impact of surface warming will be quickly overwhelmed by the polar freshening due to ice melt in the Southern Ocean. Thus, the ACC, and zonal transport more generally, is projected to slow down by around 20% by 2050.

Results

We assess changes in zonal transport in a set of three simulations from the high-resolution, 1/10th-degree ocean-sea ice ACCESS-OM2-01 model - a 'neutral' climate simulation, and two future perturbation runs. The Repeat-Year Forced simulation (sourced from (*35*)) represents a neutral climate state, and is spun up with forcings consistent with 1 May 1990 to 30 April 1991 cycling over 180 years. This simulation provides a foundational perspective of the oceanic system's behaviour without considering the effect of rapid polar melting and resulting freshening. Two future perturbation experiments (sourced from (*32*)) are branched off the RYF run, one which is forced with projected global temperature, meltwater and wind perturbations

(hereby, the *Future Perturbation* experiment), and another that is forced with projected global temperature and wind perturbations only (hereby, the *Future Perturbation without meltwater* experiment), from 1991 to 2050. The future perturbation experiments are sourced from (*32*), and the RYF simulation is from (*35*). Given the relatively high horizontal resolution of the ACCESS-OM2-01 model, these simulations capture multiple scales of ocean processes, from small-scale, sub-mesoscale eddies near the Antarctic coast, to the large-scale jets and fronts that characterise the Antarctic Circumpolar Current. The rich range of dynamics captured by the ACCESS-OM2-01 model is shown by the instantaneous snapshot of surface speed in Fig. 1. Further information on the model setup and simulations is also provided in the materials and methods section, and we refer readers to the original model papers - (*35*) and (*32*).

Broadly, the suite of ACCESS-OM2-01 simulations reveal a long-term decline in zonal transport in the Southern Ocean (as shown in Fig. 2). Understanding this declining trend is crucial for predicting broader climatic and oceanic changes in the coming decades. The time-mean zonal transport pattern in the Repeat-Year Forced (RYF) simulation shows a strong circumpolar series of jets comprising the ACC (Fig. 2a). Over the final ten years of the RYF simulation, zonal transport through the Drake Passage, and zonally-averaged zonal transport between 70-50°S is strong, at 140 Sv and 103 Sv (solid black lines in Fig. 2d and e).

Contrasting with the RYF simulation, the future perturbation simulation (averaged over the decade from 2040 to 2050) shows major shifts in zonal transport over different parts of the Southern Ocean. An increase in westward zonal transport (blue colour) is visible over the Antarctic continental slope, consistent with the location of the Antarctic Slope Current in this model (Fig. 2b). This strengthening ASC has been previously reported in a more idealised meltwater perturbation setup with the same model (*36*). In the rest of the Southern Ocean, there is an overall drop in eastward transport, signalling a decrease in Antarctic Circumpolar Current (ACC) and zonal transport. This decline is also visible in the vertically integrated

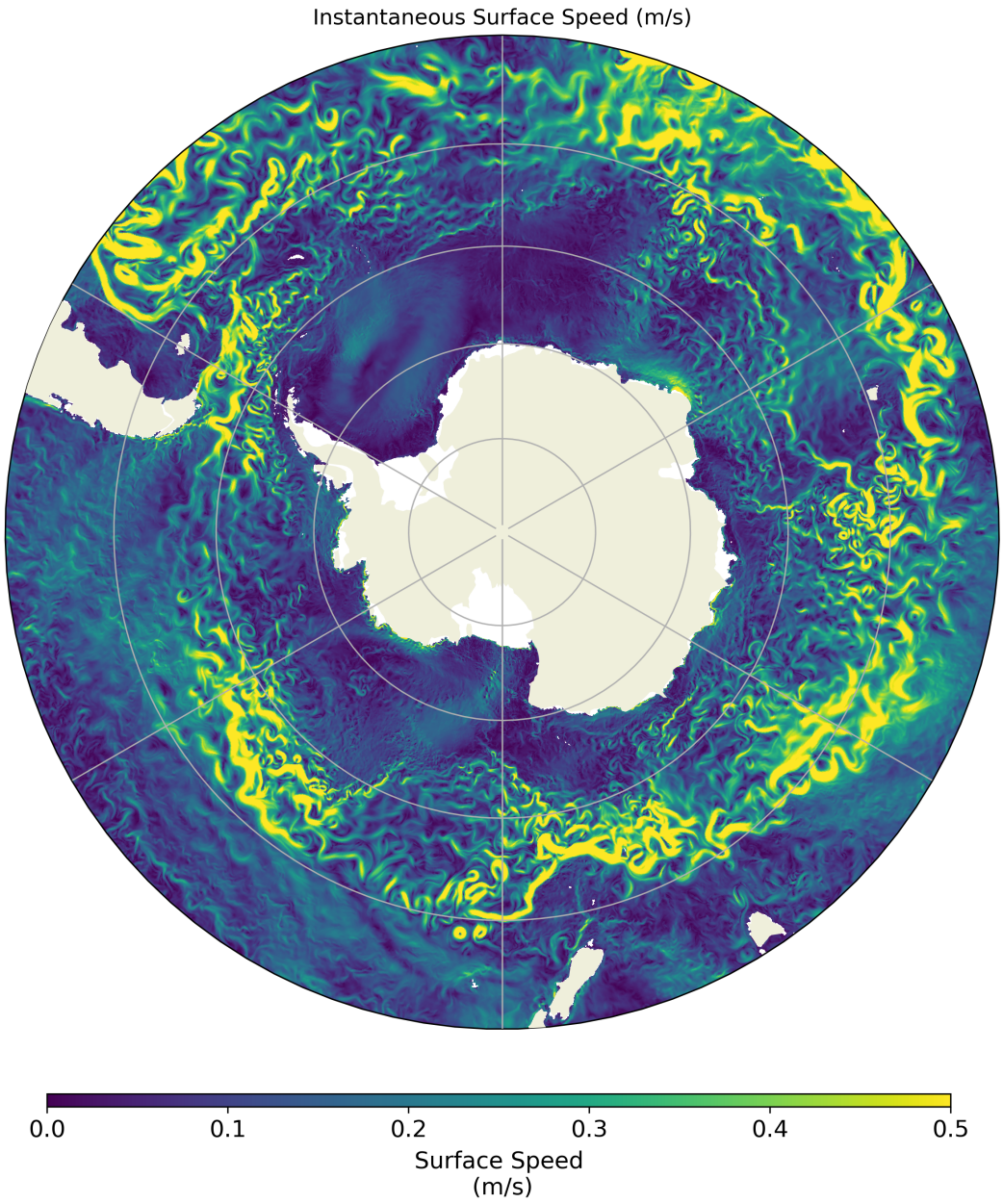

Figure 1: **Snapshot of surface speed in the ACCESS-OM2-01 model.** The daily-averaged surface speed on 31 December 1990 in the final cycle of the RYF simulation is shown.

zonal transport in Fig. 2d and e, with an approximate decrease of about 20% over four decades in both the Drake Passage and the zonally-averaged transport, calculated between 70°S and 50°S. The ACC transport (defined as the zonal transport within a range of sea surface heights

characteristic of the ACC, shown in dashed black lines in Fig. 2a-c) is also decreasing in the future simulation, as shown in Fig. 2f and g. ACC transport through the Drake Passage falls at a rate of 5 Sv/decade, and zonally-averaged falls at approximately 12 Sv/decade, again, by approximately 20%.

The future perturbation without meltwater simulation shows that this drop in ACC and zonal transport is entirely due to meltwater production around Antarctica (compare red and blue lines in Fig. 2d - g). When the model is forced solely by projected changes to winds and temperature, the zonal transport and ACC transport remains broadly unchanged. Indeed, there is a *slight* acceleration of zonal and ACC transport between 2000 and 2040 when only thermal and wind changes are used to force the model (Fig. 2e and g). This acceleration of zonal transport may be due to the same mechanisms highlighted by (*33*) - enhanced meridional thermal gradients accelerating the thermal wind transport in the Southern Ocean. However, in the model explored here, future projections of Antarctic meltwater rapidly offset this slight temperature-driven acceleration, signalling a profound shift in the dynamics controlling Southern Ocean transport.

Zonal transport in the Southern Ocean is supported by the density and stratification profiles in the water column. In order to understand the sharp drop in zonal transport over future decades, it is thus essential to understand the changes to the meridional and vertical profiles of temperature, salinity and density this part of the world. There is a fresh-to-salty, cold-to-warm, and dense-to-light zonally-averaged meridional gradient at the surface of the Southern Ocean (red lines in Fig. 3a to c). In a depth-averaged sense, however, the salinity gradient is flipped (black lines in Fig. 3a), because of the inclusion of the saltier, sub-surface Circumpolar Deep Water along the Antarctic margins, and the subducted freshwater in the Antarctic mode water further north. Nevertheless, the mean meridional gradient in density in the Southern Ocean has dense water in the south, and lighter water in the north.

The change in this mean gradient reveals the root cause of the decline in zonal transport in

the future (Fig. 3d - i). The sea surface salinity drops along the Antarctic margins (latitudes southwards of 65°S), and there is enhanced freshening in the subpolar latitudes (latitudes northwards of 65°S) consistent with the subduction of the Antarctic mode water. In deep subpolar latitudes, there is a slight trend towards increased salinity. The temperature field, on the other hand, generally warms across most regions of the ocean, with substantial increases noted in particular around the Antarctic margins. The increase in temperature around the Antarctic margins is not seen in the future perturbation without meltwater simulation (not shown), implying that the warming of the Antarctic margins here is a meltwater-driven phenomenon. The net impact of this spatially heterogeneous freshening and warming is a net lightening of the entire water column, as shown in Fig. 3f and i. The subsurface salinification of the Antarctic margins is offset effectively by the warming signal there, leading to a loss in density in the margins. Further north, warming in the mixed layer and freshening of the Antarctic mode waters combines to lighten the subsurface ocean (Fig. 3i). These shifts in temperature and salinity have significant repercussions on the overall stratification, which can influence ACC and zonal transport. This increase in top-to-bottom stratification is primarily attributed to the accumulation of freshwater near the Antarctic margin and subsurface warming in the subpolar latitudes. Similar stratification changes were showcased for the same simulations by (*32*).

Our results show that the integrated zonal and ACC transport declines in response to polar freshening. By visualising the zonally- and depth-integrated transport (Fig. 4), we explore the regions where the transport change is greatest, and the stratification changes which bring about this transport decline. In the future perturbation without meltwater simulations, there is a negligible change in depth-integrated transport south of 55°S, and an increase in zonal velocity north of 55°S (i.e., north of the Drake Passage latitudes). There is also minimal change in density, as indicated by the isopycnal lines in Fig. 4a and c. On the other hand, the future perturbation run has substantial changes in density both in the Antarctic margins and in the subpolar latitudes

(including the latitudes of the Drake Passage). The general decrease in density (compared red and black lines in Fig. 4d) is consistent with the lightening water column shown in 3i. There is a steepening of isopycnals in the Antarctic margins (i.e., increasingly negative slope), compared with a flattening of isopycnals further north. This suggests that there is an increase in geostrophic shear near the Antarctic margins, potentially enhancing the westward component of transport. Concurrently, a reduction in the eastward component of transport is inferred due to the decrease in geostrophic shear, as evidenced by the flattening of isopycnals there.

Discussion

The observed weakening of the ACC in the future perturbation simulation (from (*32*)) is a critical finding that has profound implications for understanding future oceanic and climatic changes. The reduction in ACC and zonal transport, of approximately 20% over four decades, suggests a substantial reconfiguration of Southern Ocean dynamics. This change in the ACC, one of the planet's major current systems, could have far-reaching impacts on global climate patterns, oceanic heat distribution, and marine ecosystems. The freshening of surface and subsurface waters, particularly around the Antarctic margins, and the salinification of deeper ocean layers, highlights the major alterations to the ocean's thermohaline structure that are underway. The reduced formation of Antarctic Bottom Water causes a decrease in water column density, especially in the upper layers, and plays a crucial role in global heat and nutrient distribution (*32*). Additionally, the warming signal observed in most locations, especially around the Antarctic margins, aligns with broad expectations of future ocean warming.

The rapid change in the thermohaline characteristics of the Southern Ocean in these simulations directly leads to a drop in zonal and ACC transport in the model via thermal wind balance. In fact, using a fundamental thermal wind balance-derived scaling for zonal transport for ACC-like system (*13*), we can reproduce the drop in zonal transport seen in the model. Taking the

thermal wind relationship between geostrophic velocity gradient and meridional density gradient $f\partial u/\partial z \approx (g/\rho_0)\partial\rho/\partial y$, we estimate geostrophic zonal velocity and integrated transport as $u \sim (g\Delta\rho H)/(\rho_0 f W)$ and $T \sim (g\Delta\rho H^2)/(\rho_0 f)$, respectively, where f is the Coriolis frequency, z is the vertical dimension with height H, g is the gravitational acceleration, ρ_0 is the reference density and y is the meridional dimension with width W. Now, the net change in the transport (due to the change in density gradient in the meridional direction) is estimated as:

$$\delta\mathbf{T} \sim \frac{g\delta\Delta\rho H^2}{\rho_0 f} \sim \frac{gH^2}{f}(-\alpha\delta\Delta\Theta + \beta\delta\Delta S), \tag{1}$$

where α is the thermal expansion coefficient, β is the haline contraction coefficient, Θ is the temperature, S is the salinity, δ represents the change in a property over time, and Δ represents the change in a property from south to north. We take $\delta\Delta\Theta$ and $\delta\Delta S$ from the model output (Fig. 3a and b), and assume $H = 4500$ m, $g = 9.81$ ms^{-2}, $f = -1.25 \times 10^{-4}$ s^{-1}, $\rho_0 = 1035$ kgm^{-3}, $\alpha = 10^{-4}$ K^{-1}, and $\beta = 7.5 \times 10^{-4}$ kg/g. This thermal wind-derived scaling predicts that, given a temperature and salinity change consistent with the model output, we would expect a transport change, $\delta\mathbf{T}$ of -32 Sv. This prediction is remarkably close to the integrated zonal transport change in Fig. 2e, indicating that the zonal transport in the Southern Ocean is primarily thermal wind-driven. Our scaling results solidify the conclusion that stratification changes, specifically polar freshening around Antarctica, will drive a dramatic slowdown of the ACC and zonal transport in future decades.

The schematic in Fig. 5 summarises the interaction between overturning, stratification and zonal transport that explains future changes to the ACC. Two major changes in the overturning circulation are the decrease in AABW and increase in AAIW due to the freshening from ice melting. These changes impact the water column near the Antarctic margins - there is an increase in freshwater content and stratification in the upper ocean, and a reduction in deep convection, which further reduces cold and freshwater transport to the abyss. Consequently, near

the Antarctic margins, the upper ocean becomes lighter due to freshening, while the deep ocean becomes lighter predominantly due to ocean warming (despite the slight increase in salinity there). Further northward, the upper and deep ocean warm substantially, further lightening the water column. In the upper ocean, the net effect of these changes to the water column is a steepening of the meridional density gradient, which drives an acceleration of the ACC in the upper ocean via thermal wind balance. However, the deep ocean experiences freshening (subducted by the AAIW), which compensates deep cooling and leads to negligible density change. As a result, the deep ocean density gradient becomes shallower, driving a slowdown in the ACC via thermal wind balance. The net effect of the strengthened ACC in the upper ocean, and weakened ACC in the deep ocean is an overall reduction in zonal and ACC transport. The mechanism in Fig. 5 highlights the complex processes which interact to drive a slowdown in the ACC and zonal transport in the future.

Materials and Methods

Here, we summarise the diagnostics used to analyse the zonal transport and property changes in the Southern Ocean, and provide further details on the ocean model simulations assessed. In this analysis, we assess changes to the zonal- and depth-integrated transport, and zonal- and depth-averaged temperature, salinity and density in the ocean model.

The globally-integrated (zonally-averaged) transport [in Sv], for instance, is given by

$$\mathbf{T} = \frac{\mathbf{1}}{\mathbf{\Sigma}\lambda} \iiint \mathbf{u}\mathbf{d}\phi\mathbf{d}\lambda\mathbf{d}\mathbf{z} \tag{2}$$

where u is the zonal velocity, ϕ is the latitudinal dimension, z is the depth dimension, and the integral is calculated over the longitudinal (λ) dimension. The depth-integrated (zonally-averaged) transport [in Sv/degree] is then $\mathbf{T}^{\lambda,\mathbf{z}}(\phi) = \frac{\mathbf{1}}{\mathbf{\Sigma}\lambda} \iint \mathbf{u}\mathbf{d}\lambda\mathbf{d}\mathbf{z}$, and the zonally-averaged transport [in Sv/degree/m] is given by $\mathbf{T}^{\lambda}(\phi, \mathbf{z}) = \frac{\mathbf{1}}{\mathbf{\Sigma}\lambda} \int \mathbf{u}\mathbf{d}\lambda$. We mask the zonal transport by

a range of sea surface heights before performing the above calculations to quantify the ACC transport.

The zonally-averaged thermohaline properties in the model are given by

$$\overline{C}^{\lambda}(\phi, z) = \frac{1}{\Sigma\lambda} \int C d\lambda \tag{3}$$

and depth-averaged properties may be calculated as

$$\overline{C}^{\lambda,z}(\phi) = \frac{1}{\Sigma\lambda\Sigma z} \int \int C d\lambda dz \tag{4}$$

where C is any conservative scalar property (in this case, temperature, salinity or density). These relatively simple diagnostics reveal a fundamental shift in the Southern Ocean driven by polar freshening.

Data

The primary tool used in this analysis is the ACCESS-OM2-01 ocean-sea ice model (from (*35*) and (*32*)). ACCESS-OM2-01 has a 0.1-degree horizontal resolution and has 75 vertical z^* levels. The model is composed of the MOM5.1 ocean model (*37*) coupled with the CICE5.1.2 sea ice model (*38*), and forced with the JRA55-do v1.3 atmospheric forcing product (*39*). The ACCESS-OM2-01 model significantly improves representation of dense shelf water formation and Antarctic margins processes, which directly impacts the accuracy of representation of the Antarctic Circumpolar Current (*40, 41*). The ACCESS-OM2-01 model has been analysed extensively in a variety of studies, and an exhaustive summary of the model specifics are provided in (*35*).

Three simulations are conducted using this ocean model - a Repeat-Year Forcing case (RYF), from (*35*), a future perturbation case without meltwater, which forces the ocean with projected changes to wind and temperature (only) and a future perturbation case which forces

the ocean with projected changes to wind, temperature and meltwater, both from (*32*). In the RYF case, the ocean model is forced by 55 km and a 3-hourly temporal resolution JRA55-do v1.3 forcing cycling over the 1 May 1990 to 30 April 1991 time period. This year was found to be adequately 'neutral', in that no major modes of climate variability were active during this time, by (*42*). The RYF simulation is spun up for 180 years to produce a neutral control simulation, against which the future perturbation simulations may be compared. In this work, we analyse the monthly temperature, salinity, density and zonal transport in the RYF case, time-averaged over the final 10 years (i.e. years 170 - 179) of the RYF simulation.

The two future perturbation simulations analysed in this work are set up and assessed in (*32*). In these simulations, an RYF simulation is first spun up for 200 years, as detailed above. Then, two different simulations are branched off from the RYF simulation - one with perturbed anomalous winds and thermal forcing, and one with perturbed anomalous wind, temperature and meltwater forcing fields. For the years 1991-2019, the historical JRA55-do v1.3 forcing field is used to force the future simulations, and beyond 2020, the CMIP6 high-emissions scenario, Shared Socioeconomic Pathway 5-8.5 (SSP5-8.5) is used as the model forcing field (*43*). In this analysis, we assess the monthly temperature, salinity, density and zonal transport in the future perturbation simulations, averaged over the final 10 years of the simulation (i.e., 2040 - 2050). In order to isolate the Antarctic Circumpolar Current from other dynamical processes (such as the sub-polar gyres and Antarctic Slope Current), we mask out variables outside a sea surface height mask - specifically, only zonal transport with a sea surface height between -0.35 and -1.5 meters is counted as part of the ACC. The SSH mask is calculated from the time-mean SSH field in the final ten years of the RYF simulation. This enables the calculation of both zonal transport more generally, and ACC transport specifically, from the model outputs.

References and Notes

1. S. R. Rintoul, *Geophysical Research Letters* **34**, L06606 (2007).

2. E. Rignot, S. Jacobs, J. Mouginot, B. Scheuchl, *Science Express* (2013).

3. X. L. Pan, B. F. Li, Y. W. Watanabe, *Nature Scientific Reports* **12**, 383 (2022).

4. K. Suryawanshi, B. Jena, C. C. Bajish, N. Anilkumar, *Tellus A* **75(1)**, 193 (2023).

5. A. Purich, E. Doddridge, *Commun Earth Environ* **4**, 314 (2023).

6. K. I. Ohshima, *et al.*, *Nature Geoscience* **6**, 235 (2013).

7. S. Zhou, *et al.*, *Nature Climate Change* **13**, 701 (2023).

8. C. Schmidt, A. Morrison, M. H. England, *Journal of Geophysical Research* **128**, e2023JC019774 (2023).

9. G. C. Johnson, *Journal of Geophysical Research* **113**, C05027 (2008).

10. K. A. Donohue, K. L. Tracey, D. R. Watts, M. P. Chidichimo, T. K. Chereskin, *Geophysical Research Letters* **43**, 11,760 (2016).

11. J. Marshall, K. Speer, *Nature Geoscience* **5**, 171–180 (2012).

12. A. M. Hogg, *Geophysical Research Letters* **37** (2010).

13. B. Gayen, R. Griffiths, *Annual Review of Fluid Mechanics* **54**, 105 (2022).

14. A. K. Morrison, A. M. Hogg, *Journal of Physical Oceanography* **43**, 140 (2013).

15. A. K. Morrison, M. H. England, A. M. Hogg, *Journal of Climate* **28**, 4263 (2015).

16. S. T. Gille, *Science* **295**, 1275 (2002).

17. N. P. Gillett, D. Thompson, *Science* **302**, 273–275 (2003).

18. D. W. J. Thompson, *et al.*, *Nature Geoscience* **4**, 741 (2011).

19. E. Rignot, *et al.*, *Proceedings of the National Academy of Sciences* **116**, 1095 (2019).

20. R. Goyal, A. S. Gupta, M. Jucker, M. H. England, *Geophysical Research Letters* **48** (2021).

21. R. Hallberg, A. Gnanadesikan, *Journal of Physical Oceanography* **31**, 3312 (2001).

22. M. P. Meredith, A. M. Hogg, *Geophysical Research Letters* **33** (2006).

23. D. Munday, H. L. Johnson, D. P. Marshall, *Journal of Physical Oceanography* **43**, 507 (2013).

24. V. Lefebvre, Y. Donnadieu, P. Sepulchre, D. Swingedouw, Z.-S. Zhang, *Paleoceanography* **27** (2012).

25. J.-B. Ladant, Y. Donnadieu, C. Dumas, *Climate of the Past* **10**, 1957 (2014).

26. R. Barkan, K. B. Winters, S. G. Llewellyn Smith, *Journal of Fluid Mechanics* **723**, 556 (2013).

27. T. Sohail, C. A. Vreugdenhil, B. Gayen, A. Hogg, *Journal of Geophysical Research* **124**, 4208 (2019).

28. A. Klocker, D. Munday, B. Gayen, F. Roquet, J. H. LaCasce, *Tellus A* **75**, 392–409 (2023).

29. D. R. Munday, I. Sauermilch, A. Klocker, J. M. Whittaker, *Paleoceanography and Paleoclimatology* **X**, X (2023).

30. A. Silvano, *et al.*, *Science Advances* **4**, eaap9467 (2018).

31. K. L. Gunn, S. R. Rintoul, M. H. England, M. M. Bowen, *Nature Climate Change* **13**, 537 (2023).

32. Q. Li, M. England, A. Hogg, S. Rintoul, A. A Morrison, *Nature* **615**, 841–847 (2023).

33. J.-R. Shi, L. D. Talley, S.-P. Xie, Q. Peng, W. Liu, *Nature Climate Change* pp. 1–8 (2021).

34. M. Gutierrez-Villanueva, T. Chereskin, J. Sprintall, *Nature Communication* **14**, 7792 (2023).

35. A. E. Kiss, *et al.*, *Geoscientific Model Development* **13**, 401 (2020).

36. R. Moorman, A. K. Morrison, A. M. Hogg, *Journal of Climate* **33**, 6599 (2020).

37. S. M. Griffies, *GFDL Ocean Group Tech. Rep.* **7**, 620 (2012).

38. E. Hunke, *et al.*, CICE, the Los Alamos sea ice model, *Tech. rep.*, Los Alamos National Lab.(LANL), Los Alamos, NM (United States) (2015).

39. H. Tsujino, *et al.*, *Ocean Modelling* **130**, 79 (2018).

40. A. K. Morrison, A. M. Hogg, M. H. England, P. Spence, *Science Advances* **6**, eaav2516 (2020).

41. W. G. C. Huneke, A. K. Morrison, A. M. Hogg, *Journal of Physical Oceanography* **52**, 347 (2022).

42. K. Stewart, *et al.*, *Ocean Modelling* **147**, 101557 (2020).

43. B. C. O'Neill, *et al.*, *Geoscientific Model Development* **9**, 3461 (2016).

Acknowledgments

The authors thank the Consortium of Ocean and Sea Ice Modelling in Australia (COSIMA) and the authors of (*32*) for making available the ACCESS-OM2-01 RYF and future projection simulation outputs. We particularly thank Matthew England and Qian Li for producing and supplying the future perturbation experiments for analysis. ARC Future Fellowship Grant FT180100037 supported B.G.. T.S. and B.G. were supported by the Australian Center for Excellence in Antarctic Science (ACEAS; grant number SR200100008). A.K. acknowledges support from the Research Council of Norway-funded project KeyPOCP (grant number 328941). Analysis was conducted with National Computational Infrastructure (NCI) facilities, supported by the Australian Government. The authors thank Andy Hogg for their constructive feedback on this research.

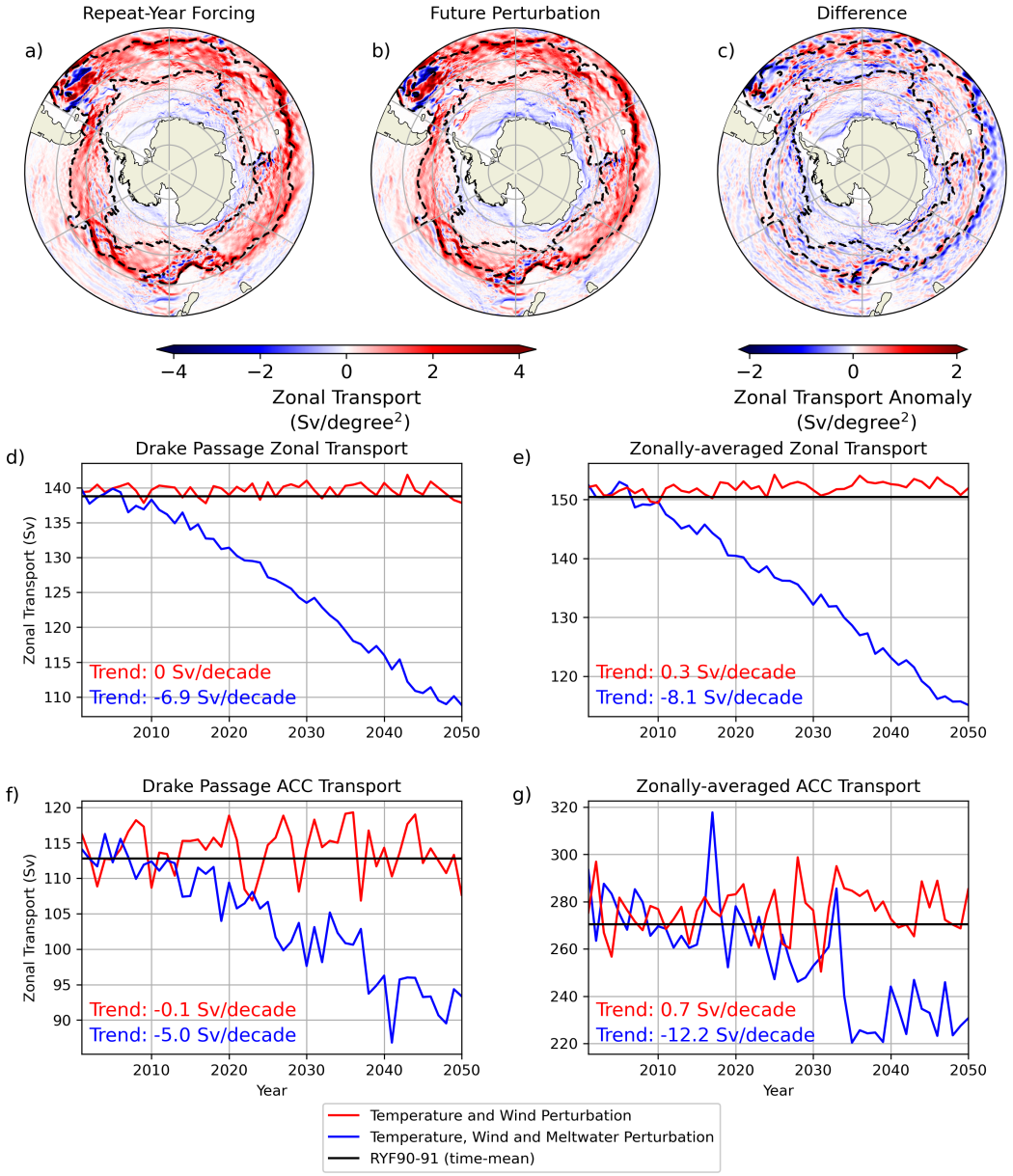

Figure 2: **Zonal transport in simulations of the ACCESS-OM2-01 model.** a) Time-mean, vertically-integrated zonal transport in the Repeat-Year Forced (RYF) simulation (averaged over the final ten years of the simulation), b) Time-mean, vertically-integrated zonal transport in the future perturbation simulation of (*32*), averaged over the 2040-2050 time period, and c) the difference in zonal transport between the future perturbation and the RYF simulation. Annual-averaged zonal transport d) through the Drake Passage, and e) zonally-averaged between 70-50°S, in the future perturbation simulation (blue line), the future perturbation *without* meltwater (red line) and time-mean transport in the RYF simulation (solid black line; averaged over the final ten years of the simulation). Annual-averaged Antarctic Circumpolar Current (ACC) Transport (as defined by the dashed black sea surface height mask in a-c) f) through the Drake Passage, and g) zonally-averaged, as above.

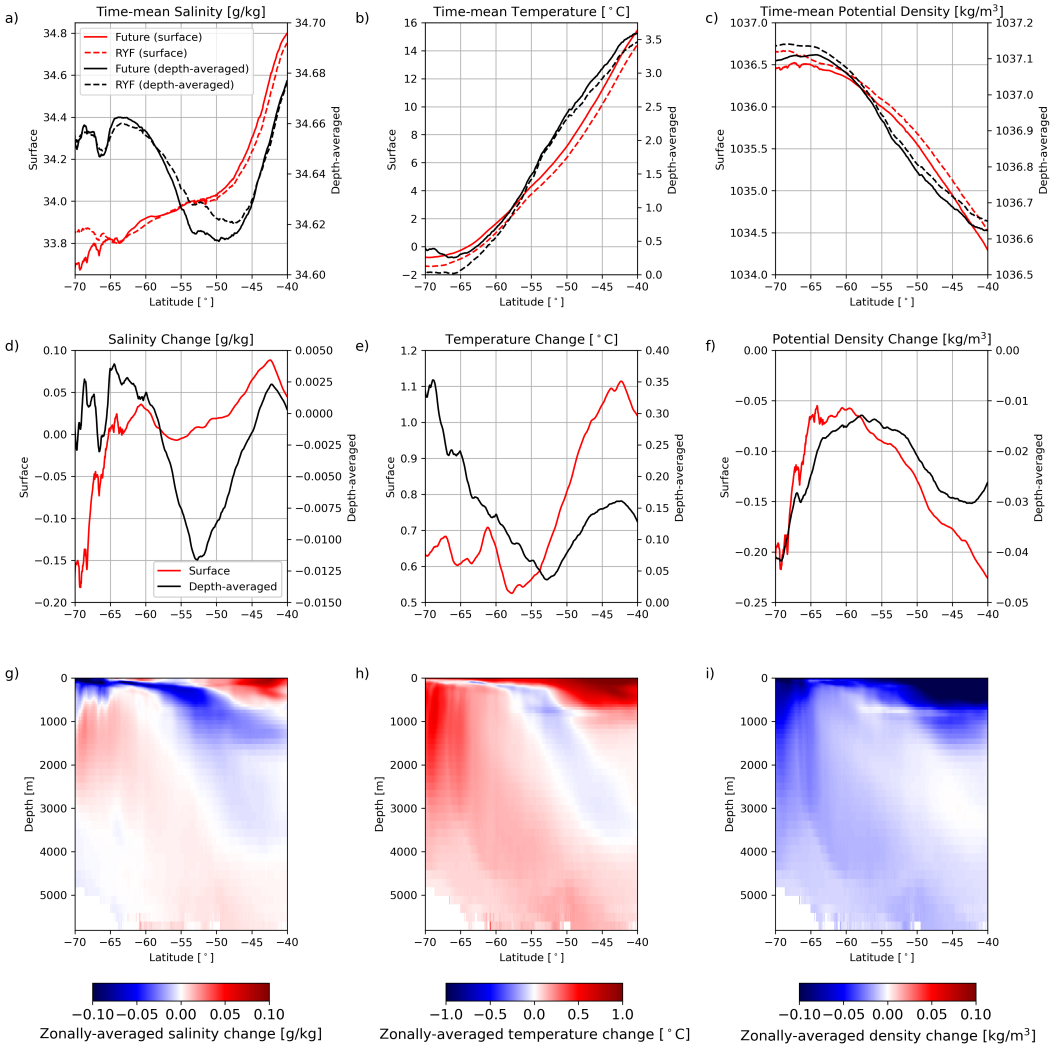

Figure 3: **Summary of the temperature, salinity and density properties of the Southern Ocean in the suite of simulations conducted.** Time-mean surface (red lines) and depth-averaged (black lines) a) salinity, b) temperature and c) density in the RYF (dashed lines) and future perturbation (solid lines) simulations. Change in surface (red lines) and depth-averaged (black lines) d) salinity, e) temperature and f) density between the RYF (time-mean over the final ten years of simulation) and future perturbation simulation (time-mean between 2040 and 2050). Zonally-averaged change in g) salinity, h) temperature and i) density between the RYF and future perturbation simulation.

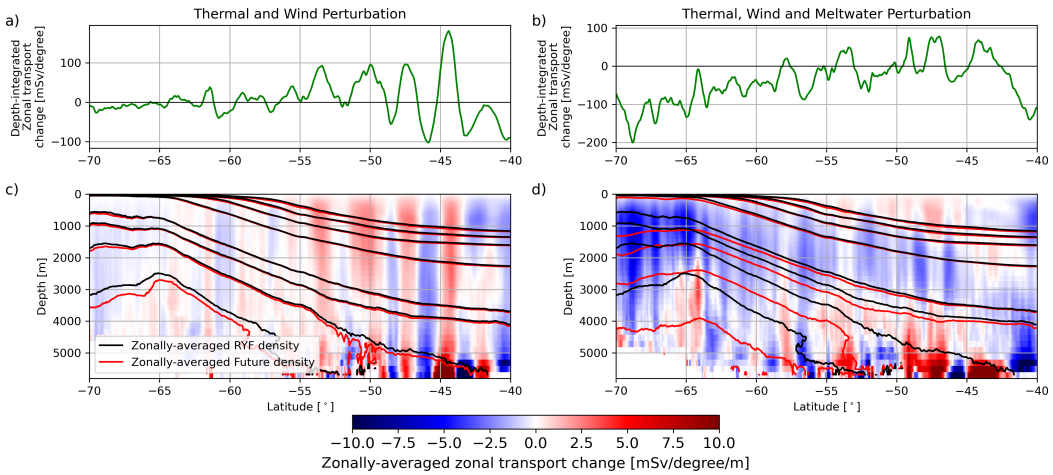

Figure 4: **Zonal transport change between the RYF and future perturbation simulations.** a) Depth-integrated zonal transport change in the future perturbation (without meltwater) simulation, b) Depth-integrated zonal transport change in the future perturbation simulation, c) zonally-integrated zonal transport change in the future perturbation (without meltwater) simulation and d) zonally-integrated zonal transport change in the future perturbation simulation. Red and black contour lines in panels c and d show selected time-mean densities in the RYF (black) and future (red) simulations.

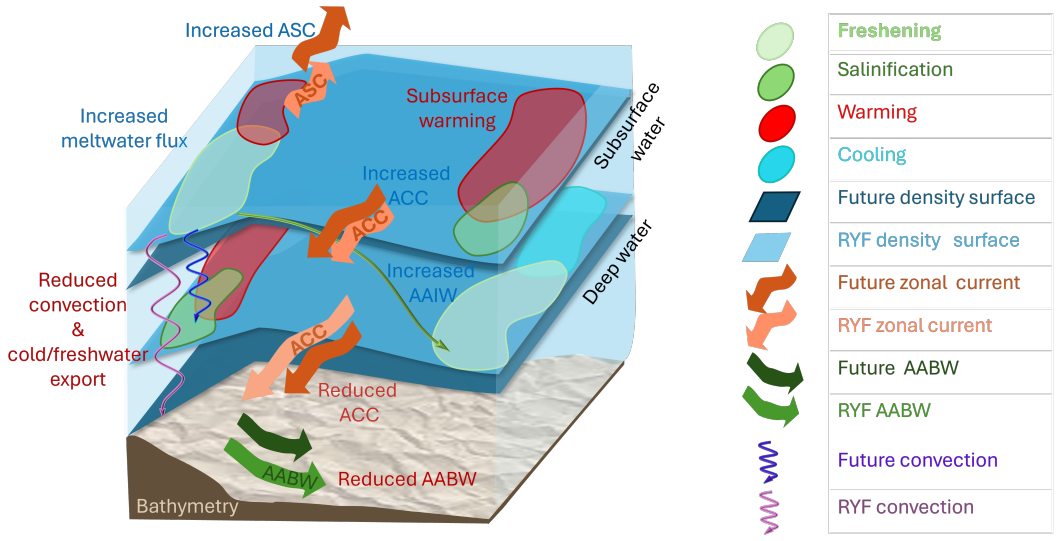

Figure 5: **Schematic of changing Southern Ocean zonal transport and its link to ocean overturning and stratification.** Water mass changes are driven by rapid freshening of the Antarctic margins and the warming of most of the water column in the future. Freshening/salinification and warming/cooling are shown by light/dark green and red/light blue patches, respectively. Arrows show the transport in the RYF and future perturbation simulations, and curly arrows mark changes to deep convection. The density iso-surfaces in the RYF and future perturbation experiment are shown in lifgt and dark blue, respectively.